photonics

MDPI

Article

Research on the Optoelectronic and Thermal Characteristics of High-Power-Density LEDs

Yihao Ma, Chuanbing Xiong *, Xirong Li, Yingwen Tang, Hui Yuan, Xinyu Yang, Bulang Luo and Jiaxin Di

College of Physics and Information Engineering, Minnan Normal University, Zhangzhou 363000, China; g2023092010@stu.mnnu.edu.cn (Y.M.); lxr1699@mnnu.edu.cn (X.L.); tyw1737@mnnu.edu.cn (Y.T.); yh1738@mnnu.edu.cn (H.Y.); g2023092001@stu.mnnu.edu.cn (X.Y.); g2024092005@stu.mnnu.edu.cn (B.L.); g2025091028@stu.mnnu.edu.cn (J.D.)

* Correspondence: chuanbingxiong@126.com

Abstract

High-power-density LED devices have emerged as a prominent focus in current research and industrial development, largely due to their role in advancing LED lighting technologies. At high power and high current, the structure and area of the thermoelectrically separated copper substrate connected to the LEDs significantly influence the device's optoelectronic performance, yet detailed studies in this area remain limited. To address this issue, blue and white LED devices with a maximum power rating of 400 W were fabricated and soldered onto copper substrates with diameters of 20 mm, 25 mm, and 32 mm. The influence of substrate area on the I–V and I–L characteristics of the LEDs was systematically measured and analyzed at different operating temperatures. Additionally, variations in operating voltage and luminous intensity with temperature were investigated under specific driving currents. Infrared thermal imaging was employed to examine the thermal field distribution under varying substrate sizes and current levels. The results show that increasing the copper substrate diameter from 20 mm to 25 mm and further to 32 mm leads to a significant improvement in LED optoelectronic performance. To determine the diameter threshold beyond which performance gains diminish, a 3D COMSOL 6.1. model was developed. The model reveals that expanding the diameter from 32 mm to 35 mm results in only a marginal improvement, while further increasing it to 40 mm offers a negligible additional benefit, thereby identifying the optimal substrate area for performance saturation.

Keywords: high-power-density LED; thermoelectric separation copper substrate; optimal substrate area

Check for updates

Received: 3 December 2025
Revised: 2 January 2026
Accepted: 5 January 2026
Published: 8 January 2026

Copyright: © 2026 by the authors. Licensee MDPI, Basel, Switzerland. This article is an open access article distributed under the terms and conditions of the Creative Commons Attribution (CC BY) license.

1. Introduction

The semiconductor lighting industry, with LEDs as the core device, is one of the most promising high-tech industries worldwide [1]. Compared with traditional light sources, high-power LEDs are known for their higher reliability and longer service life under normal working conditions [2]. High-power LEDs have the advantages of high light output, high light efficiency, long life, etc. They are widely used for underwater lighting, display lighting, safety lighting, and other fields, which is of great research value and economic benefit [3–5].

The high energy storage capacity and fast charge and discharge capability of lithium-ion batteries provide stable energy support for high-power LEDs and SiC/GaN devices. And the excellent power conversion characteristics of SiC/GaN devices reduce the energy loss of the system, thereby extending battery life and improving the drive efficiency of LEDs.

LED devices, lithium-ion batteries, and SiC/GaN MOSFETs work together to promote development, pushing semiconductor lighting technology to a new stage of development. This not only promotes innovation in the field of lighting but also lays a solid foundation for applications beyond lighting (such as visible light communication, health lighting, etc.) [6–8]. In many application scenarios in the current lighting field, LED devices and MOS tube devices need to withstand the huge currents of lithium-ion batteries, which is equivalent to the direct conduction current of LEDs. A single LED device needs to work stably at hundreds of watts of power and nearly 100 amps of current, meaning that LEDs play an important role beyond the lighting industry, such as in police flashlights and marine fisheries. This brings new development opportunities for the entire lighting industry chain.

Low-power LEDs can be effectively managed through a simple heat dissipation mechanism because of their low power consumption and limited heat generation. But the heat flux of high-power LED chips is as high as 250–500 W/cm^2 [9]. Therefore, effective thermal management techniques are essential. Generally, there are two kinds of heat conduction paths for high-power LEDs. One is packaging and heat dissipation. Through the selection of the chip, bonding layer, substrate, and other materials, the thermal resistance between the chip and interface is optimized. The other is heating sink heat dissipation, which combines the substrate with external heat dissipation structures (such as fins, heat pipes, fans, liquid cooling systems) to improve the heat dissipation capacity of the device.

At the system level, significant efforts are focused on enhancing heat exchanger design and employing advanced cooling mechanisms. For conventional and compact heat sinks, statistical optimization techniques like the Taguchi method combined with Analysis of Variance (ANOVA) have been effectively applied to reduce simulation costs while identifying the optimal design parameters for applications such as automotive headlights or confined lighting spaces [10]. Beyond passive air cooling, active cooling technologies are being intensively researched for high heat flux scenarios. This includes integrated ionic wind heat sinks, where electrostatic forces generate airflow without moving parts. Recent research has demonstrated the design and numerical optimization of cylindrical wire-fin-type integrated ionic wind heat sinks for cooling high-power LEDs, offering a compact and efficient thermal management solution [11]. More integrated approaches like chip-on-thermoelectric cooler packaging, which has demonstrated a 35% increase in LED output through active temperature control, also represent a promising direction for active thermal management [12]. In the field of thermal management for high-power LEDs, by employing metal-embedded printed circuit boards, Ding demonstrated a significant reduction in junction temperature and an enhancement of luminous efficiency [13]. Concurrently, at the chip and package level, research aims to reduce thermal resistance from the source. This involves developing high thermal conductivity substrates and interface materials (TIMs). For instance, a breakthrough approach using fluidized bed chemical vapor deposition to create a graphene skin on alumina powder has produced a composite TIM with significantly enhanced thermal conductivity. When applied to micro-LEDs, this TIM achieved a hotspot temperature reduction of 17.7 °C [14]. A recent study highlights the use of diamond substrates as a superior alternative to conventional metal-core boards, significantly improving LED reliability. Specifically, LEDs assembled on diamond boards demonstrated a substantially higher lifespan compared to those on standard metal-core printed circuit boards (MCPCBs), with an estimated acceleration factor indicating that the MCPCB-based LEDs aged 2.5 to 8.8 times faster under nominal conditions [15].

High-power-density LED devices are surface-mounted onto thermoelectrically isolated copper substrates using solder paste. These assemblies are then integrated with heat sinks and driver power supplies via wire bonding and combined with optical components to form final lighting products [16–18]. During operation, a significant amount of heat

is generated, which is primarily dissipated through longitudinal heat transfer. The substrate area is a critical parameter directly determining the device's thermal performance. Optimizing this area can enhance heat transfer efficiency and improve overall thermal management. However, research on the specific impact of substrate size on the photoelectrical performance of high-power LEDs remains scarce.

This paper investigates the influence of copper substrate area on the ultimate photoelectrical and thermal performance of high-power blue and white LED devices. The devices were mounted on copper substrates of three different diameters: 32 mm, 25 mm, and 20 mm. The optoelectronic characteristics were tested using an optical testing system, and the thermal behavior of these assemblies was experimentally characterized using infrared thermography and further analyzed through thermal simulation. Building upon the experimental data, this study extends the analysis by simulating two additional, larger substrate areas (beyond the physically tested sizes) through modeling. This combined experimental and simulation approach aims to deduce the ideal substrate area for optimal performance.

2. Experiment

2.1. Sample Preparation

The LED device was fabricated using a flip-chip with dimensions of 1397 μm × 1397 μm (equivalent to 55 mil × 55 mil). Each device module was formed by co-packaging twenty-five such chips onto an aluminum nitride ceramic substrate via a eutectic bonding process, referred to as P110 in this work. The eutectic bonding process was performed using an ASM-AD211 hot-arm eutectic bonder. All LED devices used in the experiment had a voltage specification of 3V with all twenty-five chips within each device connected in parallel. The device had a maximum power rating of 400 W. Its manufacturing process has been reported in detail in the literature [17–20]. The package size was 11 mm × 11 mm, with a thickness of 800 μm. The sample for studying the influence of copper substrate area on LED performance is listed in Table 1 and shown in Figure 1.

Table 1. The samples for studying the influence of the copper substrate area on the LED performance.

Sample	Copper Substrate Diameter (mm)	Device Light Color
S01	32	Blue
S02		White
S03	25	Blue
S04		White
S05	20	Blue
S06		White

The physical images of the 32 mm, 25 mm, and 20 mm diameter thermoelectric separation copper substrates of the unwelded LED device are shown in Figure 1. For conciseness, the term "copper substrate" in this work refers specifically to the thermoelectric separation copper substrate.

2.2. Sample Test

To ensure the accuracy and traceability of the measurement data, all key components of the station (including the DC power source, spectrometer, and thermal test head) were carefully calibrated prior to the experiments. The spectral data were acquired using a Hangzhou HASS-2000 spectral measurement system. The LED sample soldered onto a copper substrate, as shown in Figure 1, was prepared by attaching electrical leads. A uniform layer of thermal grease was applied to the back of the copper substrate, which

was then mounted onto a temperature-controlled copper test head using screws. The test head was cooled by a variable-temperature circulating water system. The electrical leads from the substrate were connected to the positive and negative terminals on the test head. The entire assembly was placed inside an integrating sphere and secured with bolts. The integrating sphere was connected to the spectrometer via an optical fiber. The LED was driven by a DC constant current power supply with an adjustable range of 0–100 A. The temperature control range of the thermocouple is 0–400 °C, and the heat dissipation of the condenser is 1150 W. The circulating water flow rate was maintained at 6 L/min, provided by a temperature-controlled bath with a volume of 100 L and a controllable temperature range of 25 to 100 °C. Figure 2 shows the measurement system for LED optical parameters.

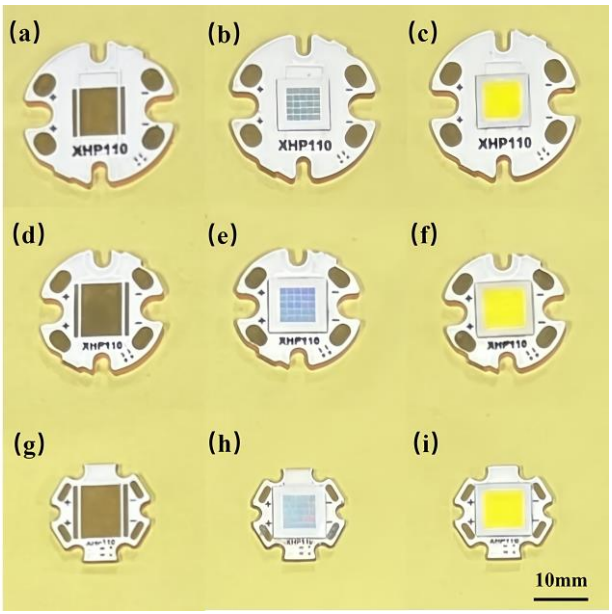

Figure 1. Physical images of the copper substrates, and the devices soldered on the copper substrate. (**a**) The 32 mm copper substrate for the P110 LED, (**b**) the P110 blue LED soldered on a 32 mm copper substrate, (**c**) the P110 white LED soldered on a 32 mm copper substrate, (**d**) the 25 mm copper substrate for the P110 LED, (**e**) the P110 blue LED soldered on a 25 mm copper substrate, (**f**) the P110 white LED soldered on a 25 mm copper substrate, (**g**) the 20 mm copper substrate for the P110 LED, (**h**) the P110 blue LED soldered on a 20 mm copper substrate, (**i**) and the P110 white LED soldered on a 20 mm copper substrate.

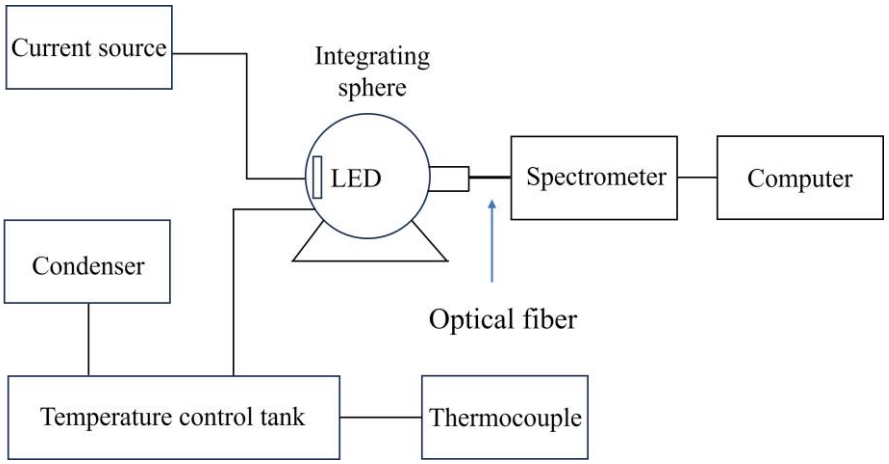

Figure 2. LED optical parameter testing system.

3. Optical Performance Test and Discussion

3.1. Blue and White Sample I–V Characteristics

Figure 3 shows the voltage–current (I-L) characteristic curve of the LED device. It can be observed that LED devices with larger substrate areas exhibited higher measured voltages. The reason for this is that as the area of the copper substrate increases, the area of the conductive copper foil also increases, and the distance between the copper substrate lead solder joints and the back electrode of the LED device also increases, resulting in an increase in series resistance. Under the same driving current, a larger series resistance will directly cause the measured voltage at both ends of the LED to rise. In addition, due to the negative temperature coefficient of LED chips, the increase in copper substrate area enhances the heat dissipation capability of LEDs, resulting in a corresponding decrease in device temperature and weakening the negative temperature coefficient of LED devices. Therefore, increasing the copper substrate area can effectively elevate the operating voltage of the LEDs.

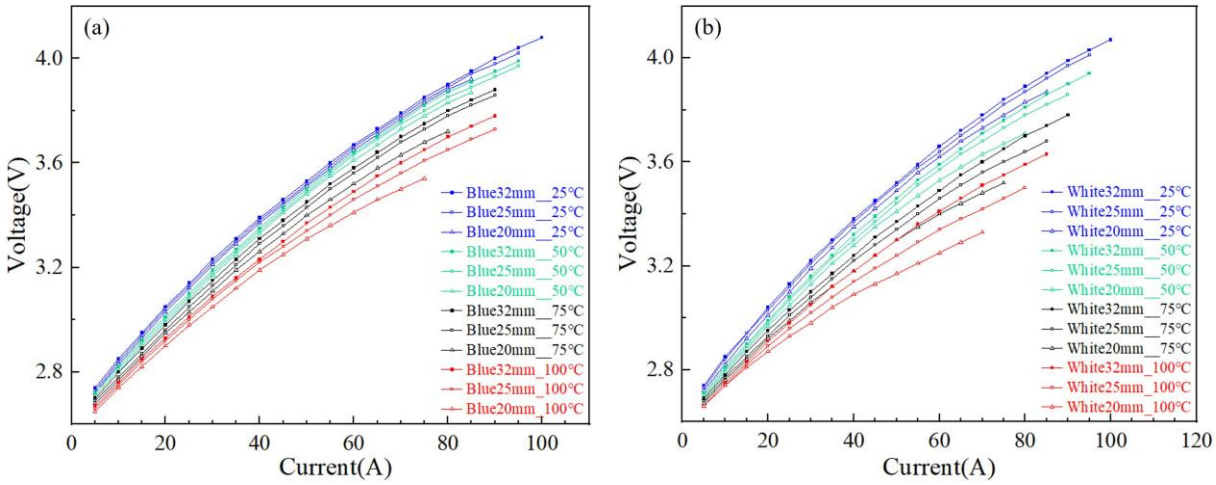

Figure 3. The change in voltage of LED with forward current under different copper substrate areas. (**a**) Blue; (**b**) white.

However, the situation is more complex for white LEDs compared to their blue counterparts. The phosphor layer undergoes thermal quenching with increasing current or temperature. This leads to a decline in the electro-optical conversion efficiency, causing more electrical energy to be converted into heat and exacerbating the temperature rise in the device. The additional temperature increase caused by the thermal effect of the phosphor layer enhances the negative temperature coefficient effect of the chip itself, resulting in a decrease in voltage. This explains the phenomenon observed in Figure 3b, where white LEDs generally exhibit a lower forward voltage than blue LEDs under identical specifications, and their I-V characteristics reach saturation earlier.

In conclusion, under conventional operating conditions, the series resistance is the predominant factor determining the variation in forward voltage with substrate area for blue LEDs. Conversely, the thermal effect, particularly the thermal quenching of the phosphor in white LEDs, serves as the key modulating factor responsible for their distinct voltage characteristics and the earlier onset of saturation compared to blue LEDs.

Figure 4 shows the LEDs with different substrate areas in the same subfigure at the same temperature. For the blue LED samples, reducing the substrate diameter from 32 mm to 25 mm and 20 mm resulted in a decrease in the forward voltage increase (ΔV) of 0.04 V and 0.14 V, respectively, at 25 °C. When the temperature rose to 100 °C, the corresponding ΔV reductions were 0.05 V and 0.22 V. In comparison, for the white LED samples under the

same diameter reductions, the ΔV decreases were 0.05 V and 0.18 V at 25 °C, and 0.13 V and 0.30 V at 100 °C. Therefore, the comparative data demonstrate that the influence of substrate area on the I–V curve is more significant for white LEDs.

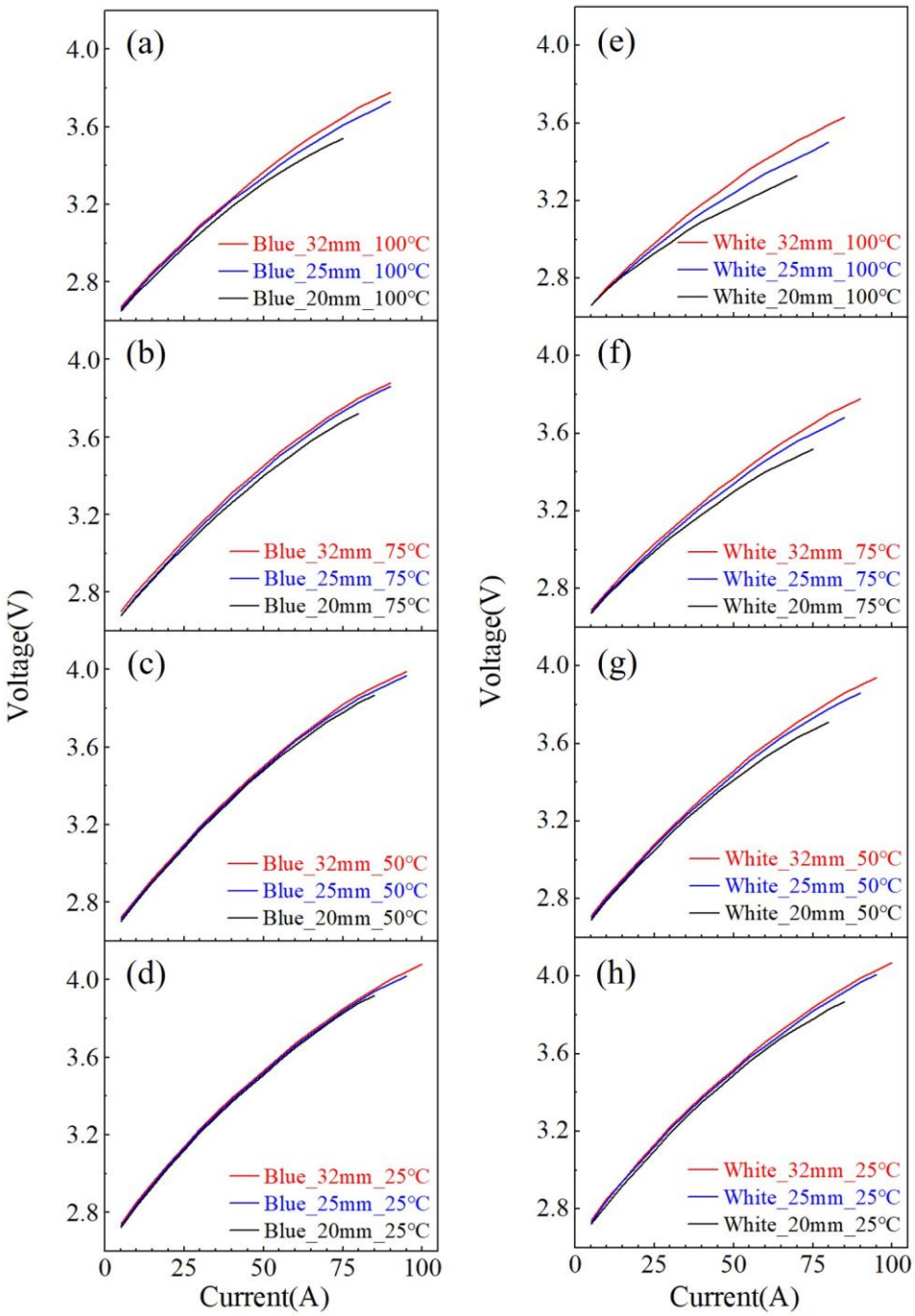

Figure 4. The change in voltage of blue and white LED with forward current under different copper substrate areas at a single temperature. (**a**) Blue at 100 °C, (**b**) blue at 75 °C, (**c**) blue at 50 °C, (**d**) blue at 25 °C, (**e**) white at 100 °C, (**f**) white at 75 °C, (**g**) white at 50 °C, and (**h**) white at 25 °C.

An increase in substrate area facilitates more uniform heat distribution across the LED, thereby mitigating the temperature-dependent influence on forward voltage. This effect is particularly pronounced at elevated temperatures, where the enhanced lateral heat dissipation in LEDs with larger substrates effectively prevents localized overheating, resulting in a minimal increase in voltage and the avoidance of voltage surges associated with hotspots. Consequently, LEDs with larger substrate areas exhibit a more gradual

voltage rise curve compared to their smaller-area counterparts, demonstrating their superior voltage stability under varying thermal conditions.

3.2. Blue and White Sample I–L Characteristics

When the LED device is powered on, it simultaneously emits light and generates heat. For end-user applications that require only brief illumination, the heat produced during short-term operation is significantly less than the heat capacity of the radiator. Consequently, this does not lead to a substantial temperature rise in the operating environment. Therefore, the room-temperature current–luminance (I–L) characteristics of the device provide clear and direct guidance for designing such application products. In contrast, when the device must operate continuously or for extended periods, the accumulated heat can approach the thermal equilibrium limit of the radiator, causing the LED to stabilize at a specific junction temperature. The equilibrium temperature is directly influenced by the radiator's design. Thus, the variable-temperature I–L characteristics not only reveal how thermal management conditions affect device performance but also offer critical insights for thermal design in practical scenarios. This constitutes a key technical rationale for investigating variable-temperature I–L characteristics in this study. Figure 5 presents the variable-temperature current–luminance (I–L) curves for the blue and white LED devices. The I–L characteristics of the two devices were measured and compared after being mounted on three copper substrates of different areas, with the temperature of the water-cooled heat radiator at 25 °C, 50 °C, 75 °C, and 100 °C.

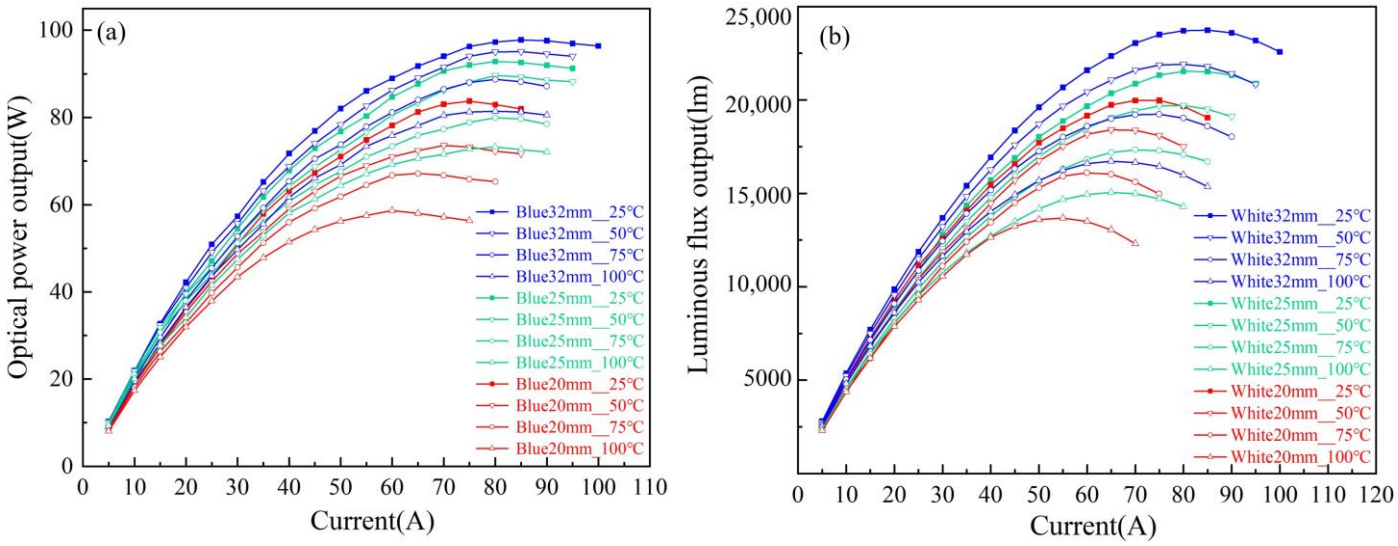

Figure 5. The change in light power of LED with forward current under different copper substrate areas. (**a**) Blue; (**b**) white.

The I–L curve of the LED exhibits a characteristic three-stage trend: a rapid initial increase, followed by a gradual rise, and ultimately a subsequent decline. At low injection currents, the probability of radiative recombination for electrons and holes within the active region is high. This results in a steep, linear increase in the I–L curve, where the external quantum efficiency approaches its peak value. As the current further increases, heat accumulation within the device leads to a significant rise in the LED junction temperature. Consequently, the rate of luminance increase with current slows down markedly, resulting in a reduced slope of the I–L curve. Beyond the peak optical output, the luminous intensity decreases with further increases in the current. This roll-off phenomenon is particularly pronounced in white LEDs. The conversion efficiency of the phosphor layer drops sharply at elevated temperatures, and a portion of the generated heat is conducted back to the LED

chip. This thermal feedback exacerbates the efficiency roll-off, leading to an overall decline in light output.

The I–L characteristics of white LEDs differ fundamentally from those of blue LEDs. White LEDs exhibit a more pronounced decline in luminous flux after reaching saturation. The primary reason for this is the significant thermal quenching of the phosphor's quantum conversion efficiency at high temperatures, causing more energy to be dissipated as heat within the package. Additionally, the photoluminescence intensity of the phosphor saturates when the excitation density from the blue pump chip reaches a critical level. Therefore, the overall luminous flux saturation of a white LED represents a superposition of the limitations imposed by both the blue chip and the phosphor layer. It is generally observed that the phosphor saturates first, followed by the blue chip, which collectively results in a lower saturation current for the white LED device compared to its blue counterpart [21–23].

For identical chips bonded to substrates of a different area, the LED mounted on the larger substrate exhibits higher luminous intensity. Increasing the substrate area enhances lateral heat spreading, which lowers the device's operating temperature. This improvement in thermal management leads to higher luminous efficiency and greater optical output power. This phenomenon is particularly pronounced in white LEDs, primarily due to the additional thermal sensitivity and efficiency roll-off of the phosphor conversion layer.

3.3. Effect of Increasing Temperature on Voltage Maintenance Rate of Blue and White LED Chips

Figure 6 depicts the variation in forward voltage with temperature for blue and white LEDs mounted on copper substrates of different areas. At a fixed drive current, LEDs on larger substrates exhibit a higher forward voltage. Furthermore, this voltage disparity between substrates of different sizes becomes more pronounced as the drive current increases. These observations serve as direct experimental evidence for the conclusion presented earlier: an increased substrate area leads to a higher LED operating voltage. Additionally, the more severe heating of the phosphor layer at higher currents results in a consistently lower forward voltage for white LEDs compared to their blue counterparts under identical conditions.

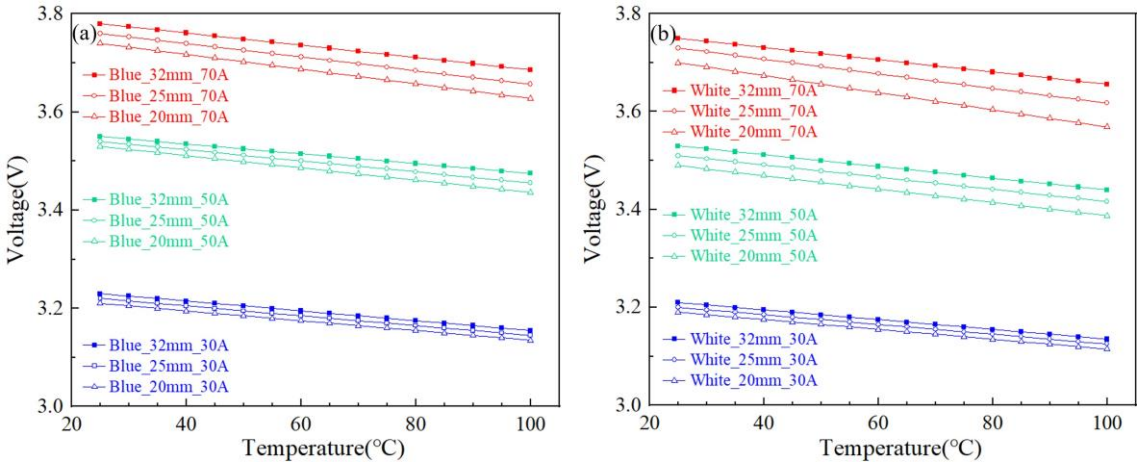

Figure 6. The change in voltage maintenance rate of LED with forward current under different copper substrate areas. (**a**) Blue; (**b**) white.

At a current of 30 A, the voltage drop rate was identical for the three substrate specifications and was the same for both blue and white LEDs. The initial voltage difference between the 20 mm and 32 mm samples was 0.02 V. When the current increased to 50 A, the voltage drop rate became greater than that at 30 A for all substrates. Notably, the voltage of the white LED samples decreased more rapidly, which is attributed to additional

heating from the phosphor layer. At 70 A, the thermal demands on the device increased further, amplifying the influence of substrate area on voltage. The maximum voltage difference between 20 mm and 32 mm LED samples reached 0.09 V at 100 °C. These results demonstrate that optimizing thermal management is crucial in high-power LED design to ensure stable high-temperature operation, extend service life, and improve long-term reliability.

3.4. Effect of Increasing Temperature on Lumen Maintenance Rate of Blue and White LED Chips

Figure 7 presents the relative luminous flux maintenance of blue and white LEDs fabricated on copper substrates of varying areas. To facilitate a direct comparison of the thermal stability trends, the luminous flux (or optical power for blue LEDs) at each elevated temperature was normalized to its value at 25 °C (baseline data provided in Table 2).

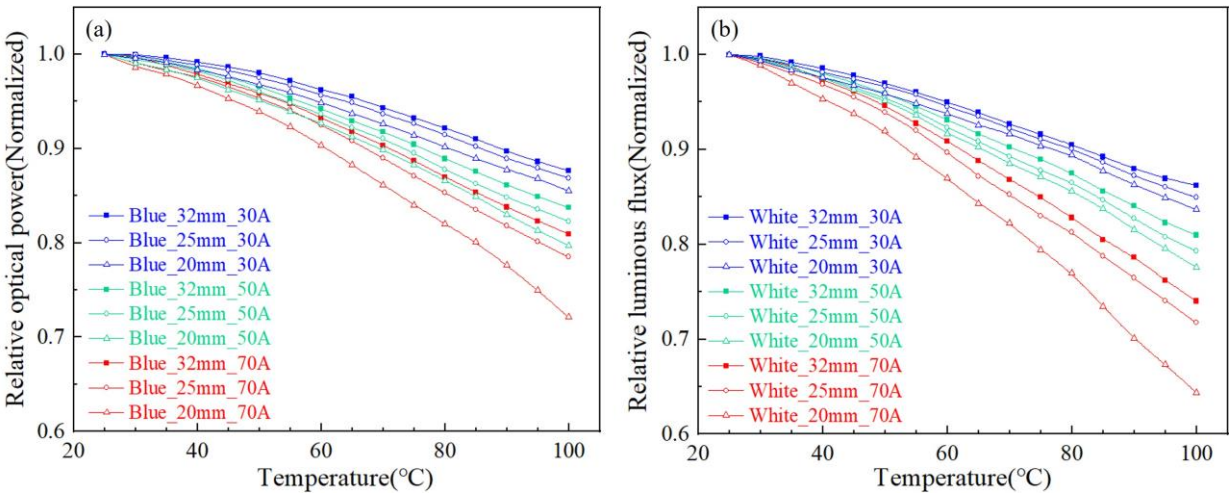

Figure 7. The change in relative optical power or luminous flux of LED with forward current under different copper substrate areas. (**a**) Blue; (**b**) white.

Table 2. LED devices at 25 °C of optical power or luminous flux.

Device Light Color	Copper Substrate Area (mm)	Current (A)	Maximum Luminous Power (W)	Maximum Luminous Flux (lm)
Blue/White	32	30	57.34	13,688
	25		54.52	12,797
	20		51.18	12,442
	32	50	82.04	19,613
	25		76.47	18,025
	20		71.01	17,710
	32	70	95.03	23,051
	25		90.93	20,872
	20		83.03	19,969

At a current of 30 A, the temperature had little influence on the luminous efficiency, and the relative luminous efficiency was above 80%. But the difference between the LED luminous efficiency of 32 mm and 25 mm substrates was smaller than the LED luminous efficiency of 25 mm and 20 mm substrates. The blue light devices of 32 mm and 25 mm differed by 0.5%, the 25 mm and 20 mm differed by 2.6%, while the 32 mm and 25 mm white devices differed by 0.8% and the 25 mm and 20 mm differed by 1.3%. This shows that the increase in the substrate area has the effect of improving the heat dissipation performance, and the increase in the substrate area improves the transverse heat dissipation capacity of the device. When the current increased to 50 A, the luminous efficiency difference between the three specifications of devices increases, and the white light device decreased faster than the blue light. The phosphor generates heat during the test, resulting in more of the

energy being released as heat. At 70 A, the 20 mm substrate had a significant gap with the other two specifications of the substrate. The luminous efficiency of the blue light device with a substrate area of 20 mm at 100 °C was 72% of that at 25 °C, while the white light device was 64%, and the heating phenomenon was serious at this time.

4. Thermal Performance Test and Discussion

4.1. Thermal Imaging Measurement and Calibration

The surface temperature distribution and thermal homogeneity of the LED devices under various driving currents were characterized using non-contact infrared thermography. This technique is based on detecting the infrared radiation emitted from the object surface, which is directly related to its temperature according to Planck's law. The measurements were conducted using a HIKMICRO P20 Max thermal imaging camera. The core technical specifications of the camera are detailed in Table 3 below.

Table 3. Thermal imaging instrument parameters.

Parameter	Infrared Resolution (Pixels)	Thermal Sensitivity (mK)	Spectral Range (μm)	Temperature Measurement Range (°C)	Measurement Accuracy (°C)
Specification	256 × 192	≤50	8–14	−20–550	±2

To overcome the low and non-uniform emissivity of the bare GaN-LED chip and metal electrodes, a thin, uniform layer of high-thermal-conductivity silicone grease ($\varepsilon \approx 0.95$) was applied to the chip surface prior to measurement. The camera was mounted on a stable tripod, perpendicular to the LED test surface, at a fixed working distance of approximately 5 cm. The ambient temperature was recorded as 25 ± 1 °C. For each driving current (10 A, 30 A, 50 A, 70 A), the LED was powered until thermal steady-state was reached (typically after 30 s). The raw thermal images were analyzed using the manufacturer's software.

4.2. Thermal Field Analysis

Effective thermal management within the chip is central to balancing the performance, power handling, and reliability of high-power LEDs. Inhomogeneities in the thermal field directly impact the chip's performance, reliability, and lifetime, a challenge that becomes particularly acute in advanced manufacturing and highly integrated designs. When chips are mounted on substrates of varying areas, their heat dissipation differs. This non-uniformity can lead to variations in the luminous intensity of individual chips. To achieve high optical power density for applications requiring intense, short-duration illumination (such as dazzling or remote lighting), high-power LEDs are often driven near their optical saturation limit. For instance, the blue LED on a 20 mm substrate in this study reached optical saturation at 70 A. Therefore, to systematically study heat generation under different drive conditions, four representative currents (10 A, 30 A, 50 A, 70 A) were selected.

Figures 8–10 present the thermal images of blue LED devices soldered on substrates with diameters of 32 mm, 25 mm, and 20 mm, respectively, at four current values. In these figures, BM denotes the base materials. A consistent observation across all samples is the monotonic increase in chip temperature with rising current. At lower currents (e.g., 10 A, 30 A), the temperature differences among the three substrate specifications are minimal, indicating that the generated heat is low and can be effectively dissipated by the thermal management system. As the current increases, the thermal disparity becomes pronounced. Significant heat accumulation is observed at the center of the chips, as evidenced by the brighter areas in the corresponding thermal images. The brightest spot consistently aligns with the electrode gap region at the chip's center. This localized heating can be attributed

to the thermal dissipation path. Unlike the anode and cathode eutectic regions, which are in direct contact with the ceramic substrate, the heat generated in the electrode gap region during operation cannot be dissipated vertically. It must first conduct laterally through the chip's sapphire substrate to the eutectic regions and then transfer downward through the ceramic substrate to the copper base and heat sink. Consequently, when the LED epitaxial layer within the electrode gap region is energized and emits light, its thermal dissipation condition is less efficient than in the regions directly above the eutectic bonds, resulting in a higher localized temperature at the center.

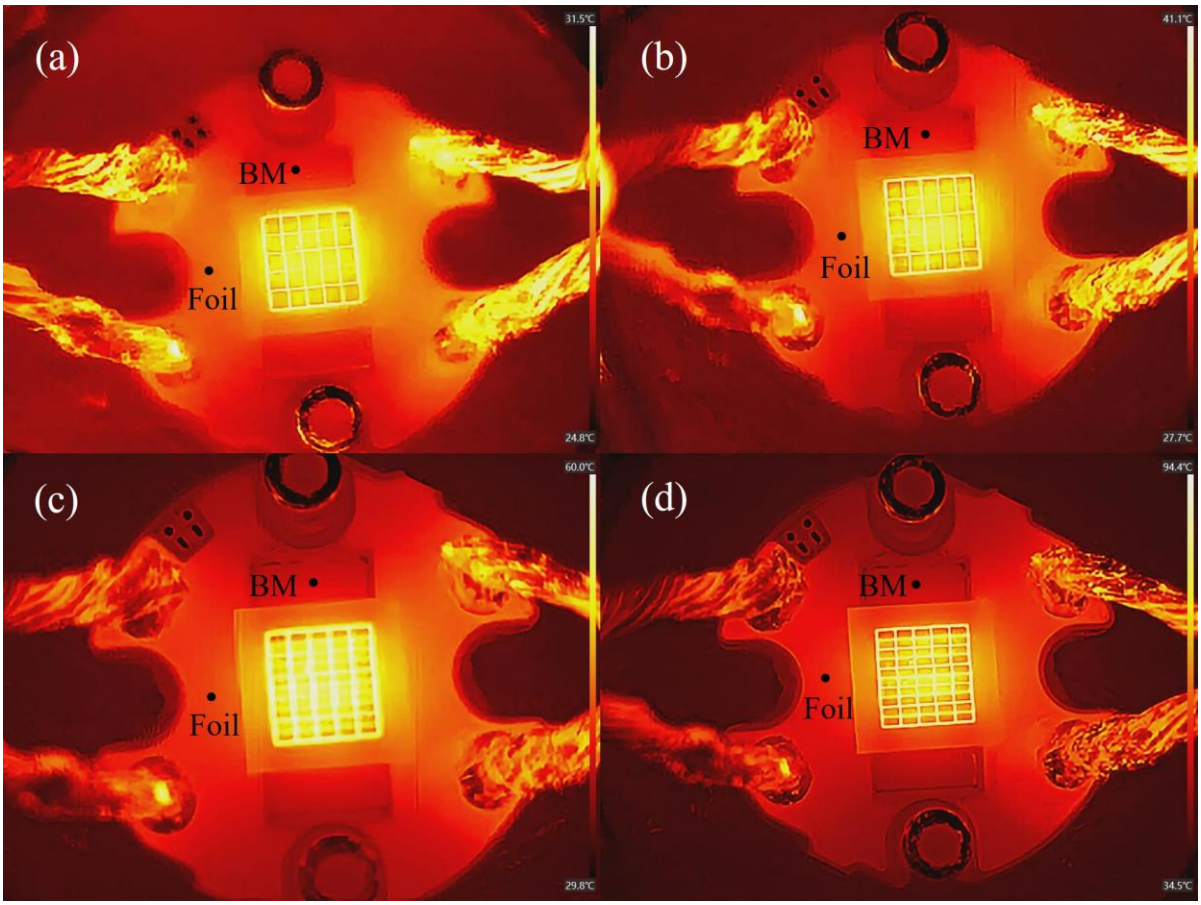

Figure 8. Thermal field of blue LED on 32 mm substrate under different currents: (**a**) 10 A, (**b**) 30 A, (**c**) 50 A, (**d**) 70 A.

When the current increases to 70 A, the inhomogeneity of the thermal field within each individual chip becomes markedly more pronounced. In inverted LED chips, the P-type conductivity is achieved through a P-type ohmic contact layer (typically a silver mirror and barrier layer metal). It is generally held that the P-type electrode of inverted LED chips does not contribute significantly to lateral current spreading issues. Conversely, the current for N-type conductive current flows into the N-type layer of the gallium nitride LED film through electrode vias, and the N-type layer has lateral resistance. An increase in current can lead to the uneven distribution of the current. Therefore, the presence of the central electrode gap in the flip-chip architecture is identified as a key factor limiting the development of high-power-density devices with a uniform optical output in ceramic packages.

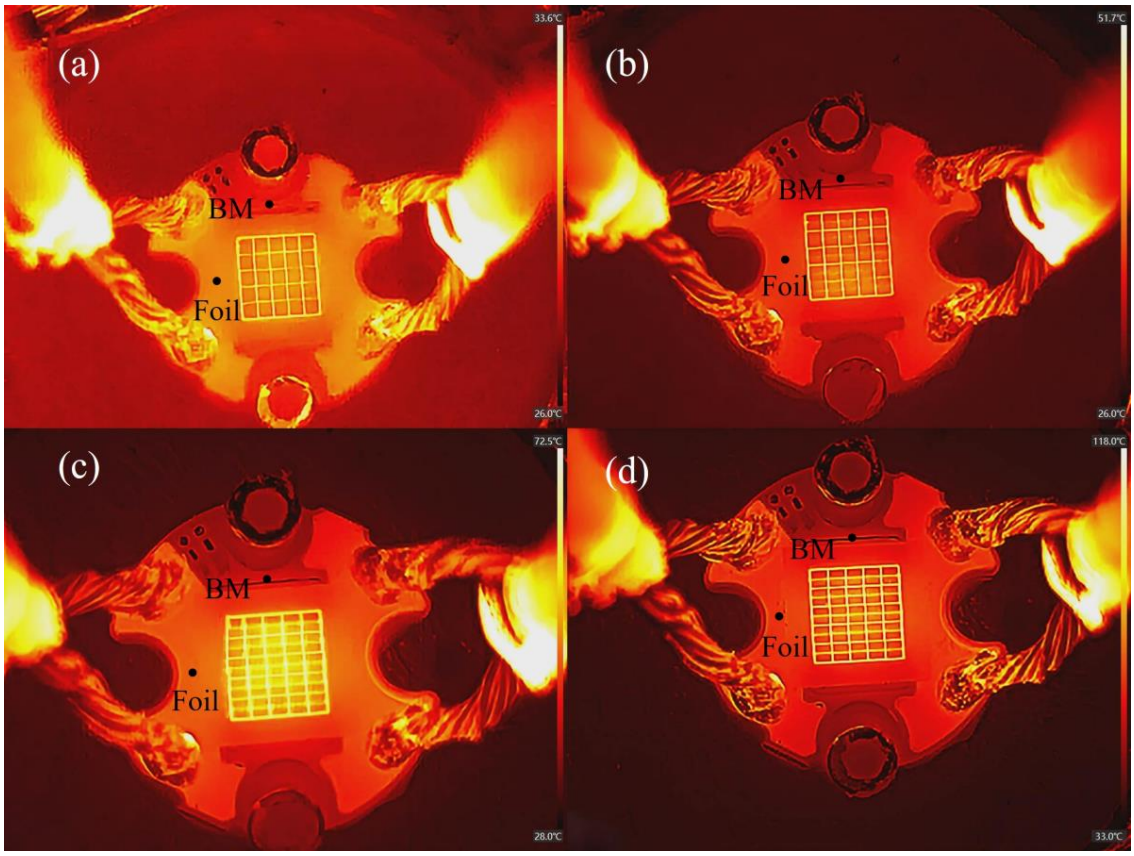

Figure 9. Thermal field of blue LED on 25 mm substrate under different currents: (**a**) 10 A, (**b**) 30 A, (**c**) 50 A, (**d**) 70 A.

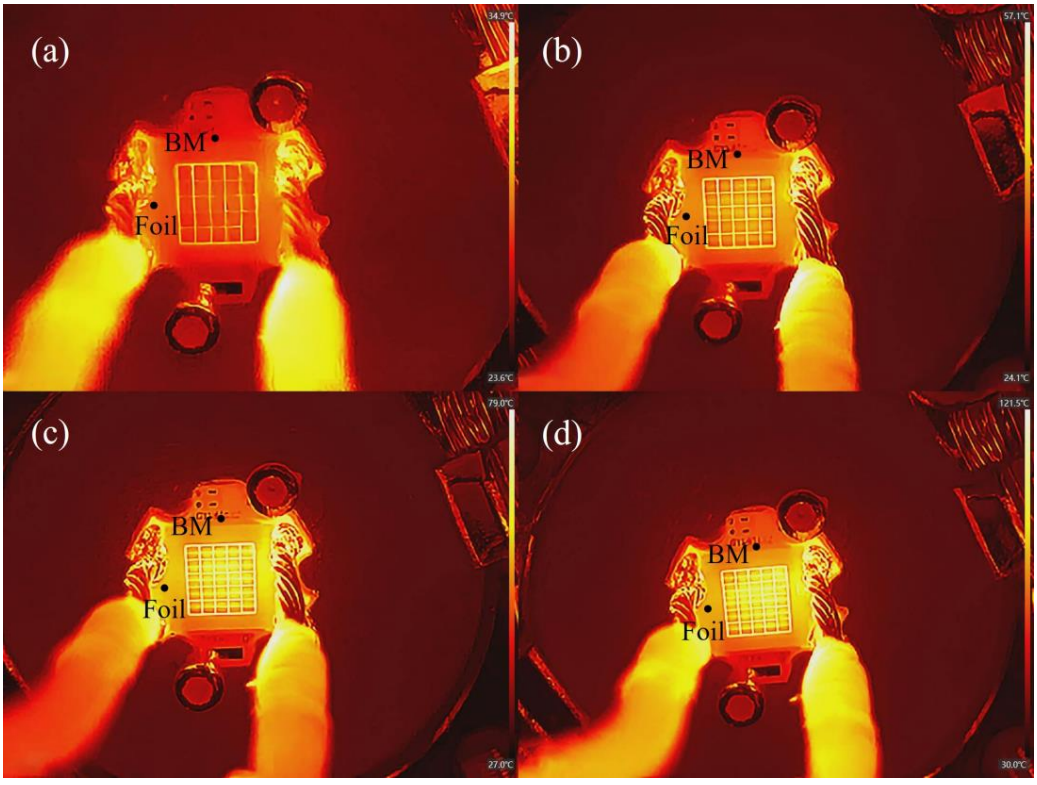

Figure 10. Thermal field of blue LED on 20 mm substrate under different currents: (**a**) 10 A; (**b**) 30 A; (**c**) 50 A; (**d**) 70 A.

Figure 11 shows a cross-sectional view of the LED device structure packaged with inverted blue light chip ceramics. When the device is powered on and emits light, the heat generated is mainly conducted to the convex part of the copper substrate through the middle PAD of the back electrode surface of the device. The heat from the convex part is then conducted laterally towards the copper substrate and transmitted to the heat sink through the thermal conductive adhesive. There is a certain thermal resistance of the thermal conductive adhesive on the longitudinal heat dissipation heat channel, which leads to the need for heat to be conducted laterally on the copper substrate. Therefore, when the substrate area increases, the lateral heat dissipation effect is strengthened, the device temperature decreases, the luminous efficiency improves, and the optical power increases.

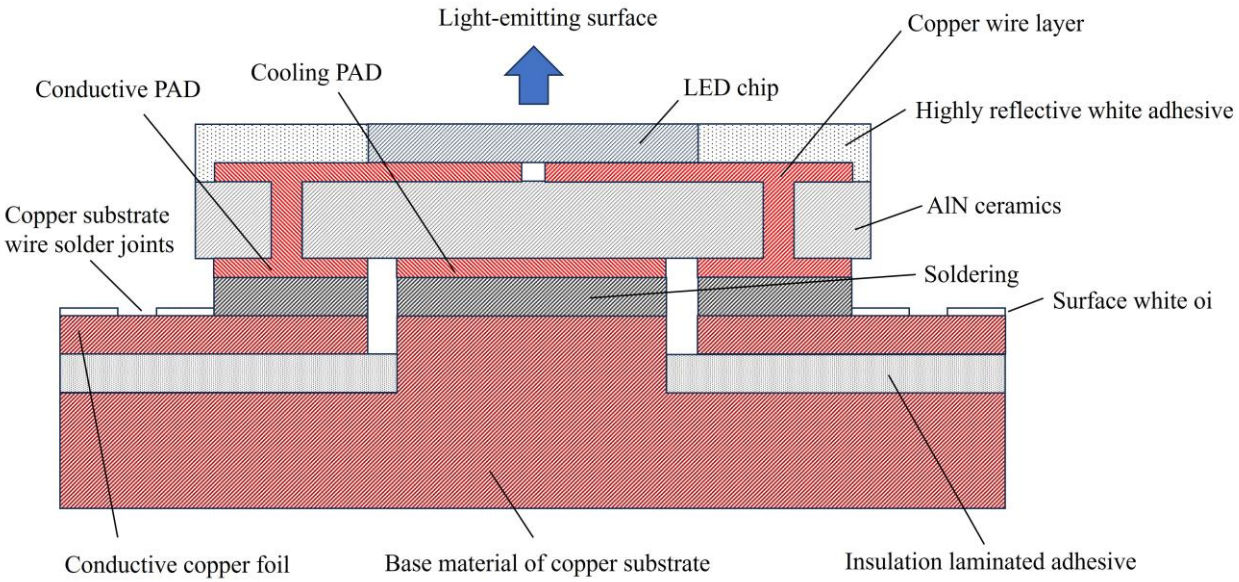

Figure 11. Structural sectional view of LED device with inverted blue chip ceramic packaging.

As the substrate area further increases, its lateral temperature gradient decreases, and the temperature difference between the expanded substrate region and the heat sink decreases, resulting in a decrease in the longitudinal thermal conductivity of the increased area. Consequently, when the substrate diameter increases from 25 mm to 32 mm, the improvement in heat dissipation capacity is smaller than that observed when the diameter increases from 20 mm to 25 mm. In practical applications, the luminescence intensity of high-power LED devices should not only consider the increase in light intensity caused by the increase in copper substrate area to improve the I-L luminescence characteristics but also take into account that as the substrate area increases, the conductive copper foil area will correspondingly increase, and the copper foil line resistance will correspondingly increase, causing changes in the I–V characteristics. Therefore, selecting the substrate area necessitates a comprehensive consideration and optimization of the interdependent optical, electrical, and thermal performance aspects.

4.3. Simulation

4.3.1. Meshing

In order to further investigate the influence of substrate area on the heat dissipation capability of LED chips, this paper used COMSOL to simulate the thermal performance of the chips. This section establishes a three-dimensional finite element thermal simulation model that fully corresponds to the experimental device. The aim is to conduct an in-depth analysis of the thermal distribution characteristics within the LED package structure under different driving currents and to investigate the influence patterns of different substrate

sizes on heat dissipation performance. The geometric model consists of the following layers from top to bottom: the phosphor layer, the LED chip, the ceramic substrate, the solder layer, the copper base plate, and the thermal grease layer. The bottom surface of the copper base plate was assigned a convective cooling boundary condition. All other external surfaces of the model were set as adiabatic to replicate the experimental insulation and minimize environmental interference. Additionally, the temperature at the copper base plate bottom was fixed at the experimental ambient temperature of 25 °C.

An unstructured mesh was generated using a physics-controlled scheme with local manual refinement. Local mesh refinement was implemented in regions of high thermal gradients, such as the chip active region and material interfaces, to accurately resolve critical thermal features. A systematic mesh convergence study was performed to ensure that the results were independent of mesh density. This involved progressively refining the global mesh while monitoring the variation in two key outputs: the maximum chip temperature and the average substrate temperature. Convergence was achieved when further refinement from approximately 560,000 elements resulted in a change in less than 1% in these parameters. All production simulations were conducted using this validated mesh configuration, which comprised about 561,379 elements.

4.3.2. Simulation Parameter Setting

The geometric model of the LED chip was constructed by retaining the main components (the chip, metal substrate, and heat sink) while omitting minor structures such as bonding wires and gold–tin solder. After completing the geometric model, it is necessary to set the material type for the specific parts of the geometric body and input the various parameters of the material, as shown in Table 4.

Table 4. Materials and parameters for different areas.

Layer	Materials	Thermal Conductivity (W/(m·K))	Layer Thickness (μm)
LED chips	GaN	130	150
Substrate	AlN	180	375
Solder paste	Sn	80	5
Tim	Silicone	3	100
Base material	Copper	401	1500
Fluorescent layer	Y_3AlO_{12}	0.5	60

4.3.3. Simulation Results

Due to the difficulty of directly measuring the thermal power of LEDs through experiments, indirect methods are used to calculate the thermal power. By accurately measuring the I-V characteristics of the chip and conducting integrated sphere flux testing, transient response errors in direct thermal measurements can be effectively avoided. This method can effectively avoid transient response errors in direct thermal measurements by accurately measuring the I-V characteristics of the chip and conducting integrated spherical light flux testing. The formula for calculating thermal power is shown in Equation (1):

$$P_T = P_E - P_L = UI - P_L \quad (1)$$

where P_T is the thermal power (W), P_E is the electrical power (W), P_L is the optical power (W), U is the voltage (V), and I is the current (A).

In the simulation, the initial ambient temperature of the substrate is set to 25 °C, and 25 blue chips are set as the heat source. The heating power is equal to the experimentally measured electrical power minus the optical power. By changing the magnitude of thermal power to meet the working state of the chip under different currents, steady-state analysis is

used to directly solve the temperature field, explore the trend of chip temperature changes, and analyze the influence of copper substrate area on chip heat dissipation.

Figure 12 shows the thermal field simulations of 32 mm, 25 mm, and 20 mm substrates under different currents. Figure 12 contains four subfigures, Figure a–d, corresponding to current sizes of 10 A, 30 A, 50 A, and 70 A, respectively.

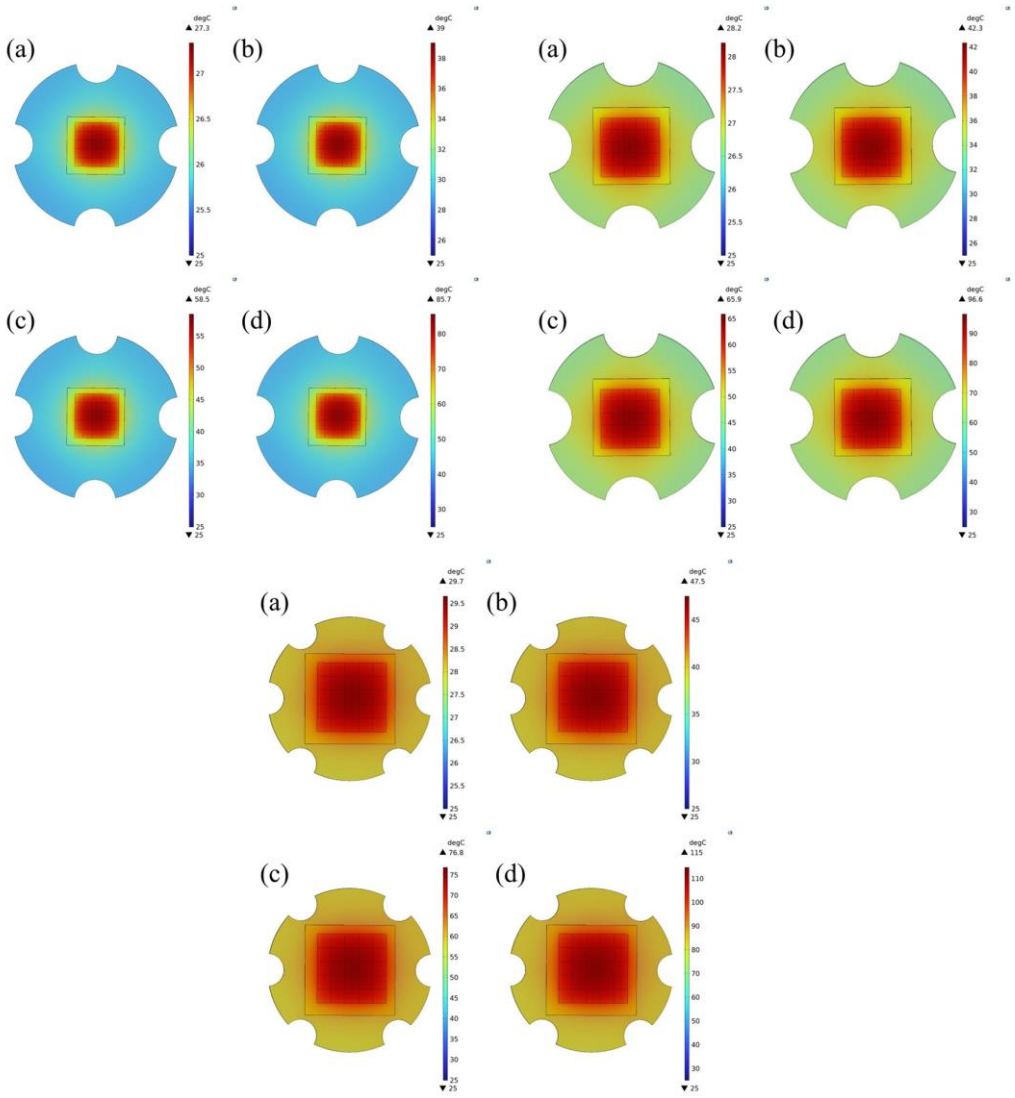

Figure 12. Thermal field simulation of blue LEDs on 32 mm (**left**), 25 mm (**right**), and 20 mm (**below**) substrates under different currents: (**a**) 10 A, (**b**) 30 A, (**c**) 50 A, (**d**) 70 A.

For the 32 mm substrate, when the current is 10 A, the chip center temperature is 27.3 °C, the red area is small, and the heat is less. With the increase in current, the peak temperature gradually increases, the maximum temperature reaches 85.7 °C at 70 A, and the red area expands significantly. The heat is mainly concentrated in the chip area and gradually diffuses outward and maintains a low temperature outside.

For the 25 mm substrate, when the current is 10 A, the center temperature is 28.2 °C, and the heat dissipation is slightly worse than that of the 32 mm substrate. With the increase in the current, the maximum temperature at 70 A is 96.6 °C, and the heat accumulation phenomenon is more serious. The color distribution has a more pronounced red concentration than the 32 mm substrate. Compared with the 32 mm substrate, the temperature in the edge area increased, and some areas changed from blue to green.

For the 20 mm substrate, when the current is 10 A, the center temperature is 29.7 °C, indicating that a smaller substrate leads to more heat accumulation. With increased power, the maximum temperature is up to 115 °C. The red area is larger, the central area of the chip is hotter, and the temperature gradient around the periphery becomes slower, and the heat cannot be effectively dissipated. The entire substrate changed from blue to yellow and orange, and the overall temperature was higher than that of the chip.

The highest temperature of the 32 mm substrate is 85.7 °C, that of the 25 mm substrate is 96.6 °C, and that of the 20 mm substrate is 115 °C. This indicates that increasing the substrate size can improve the heat dissipation capacity of the chip. The red area of the 32 mm substrate is concentrated near the chip, while the 20 mm substrate shows almost the entire area in red. Regarding the temperature variation on the periphery, the outer edge of the 32 mm substrate remains blue or green, while the outer edge of the 20 mm substrate turns yellow, with a higher overall temperature and poorer heat dissipation effect.

4.4. Comparison of Simulation and Experimental Results

Figure 13 shows the comparison between the simulation and experimental results. It can be seen that the changing trend of the measured chip junction temperature is consistent with that of the simulation results. This is because the setting of heating power in the simulation is based on the experimental data, which is more in line with the nonlinear change in the experimental data. When the current is low, the temperature in the central area of the simulation and the experiment is basically the same. The temperature difference increases as the current increases. This is because the simulation simplifies fine structures such as the welding wire, and the experiment cannot reach the ideal conditions of the simulation. The experimental test data is larger than the ideal simulation situation. The overall simulation results are consistent with the experimental results, verifying the accuracy of the COMSOL thermal model and the model establishment.

From the above experimental data and simulation data, it can be seen that it is feasible to simulate the thermal field distribution of LED chip through COMSOL, and the simulation can simulate the conditions that are not met by the experiment and further save costs.

In order to investigate the impact of further increasing the substrate area on the heat dissipation effect of the chip, the substrate area is increased to 35 mm and 40 mm, as Figure 14 shows. According to the previous experimental results, it is found that the sample heating power is about 170 W, so the heating power is set to 170 W, and the thermal field of the LED chip is observed.

When the area of the copper substrate is 35 mm, the temperature in the central region decreases by 3 °C compared with 32 mm, while when the area of the copper substrate increases to 40 mm, the temperature in the central region only decreases by 0.2 °C compared with 35 mm. This indicates that the increase in the area of the copper substrate does not increase the heat dissipation effect without restriction but instead shows a trend of saturation after reaching a certain critical point. For the characteristics of the sample studied in this paper, considering the heat dissipation performance and raw material cost, the copper substrate area of 35 mm is regarded as an optimal choice, which can realize efficient heat dissipation and effectively save raw materials.

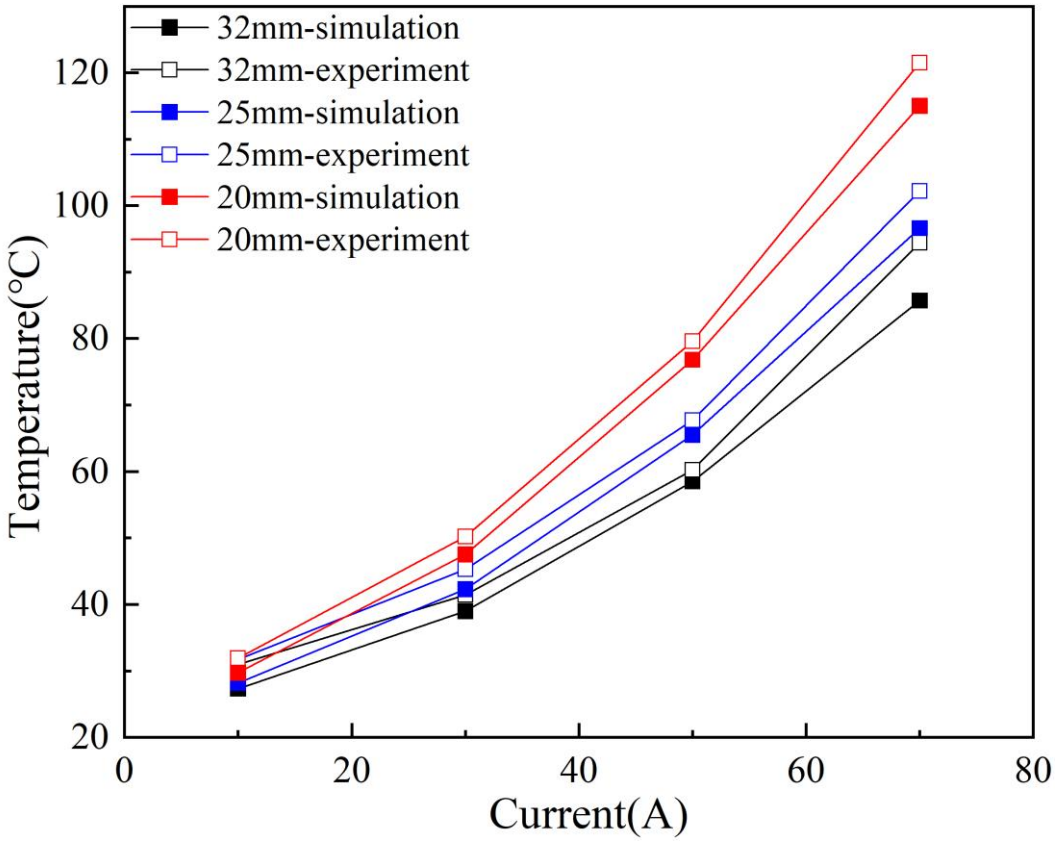

Figure 13. Comparison of simulation and experimental temperature in the central area of the chip.

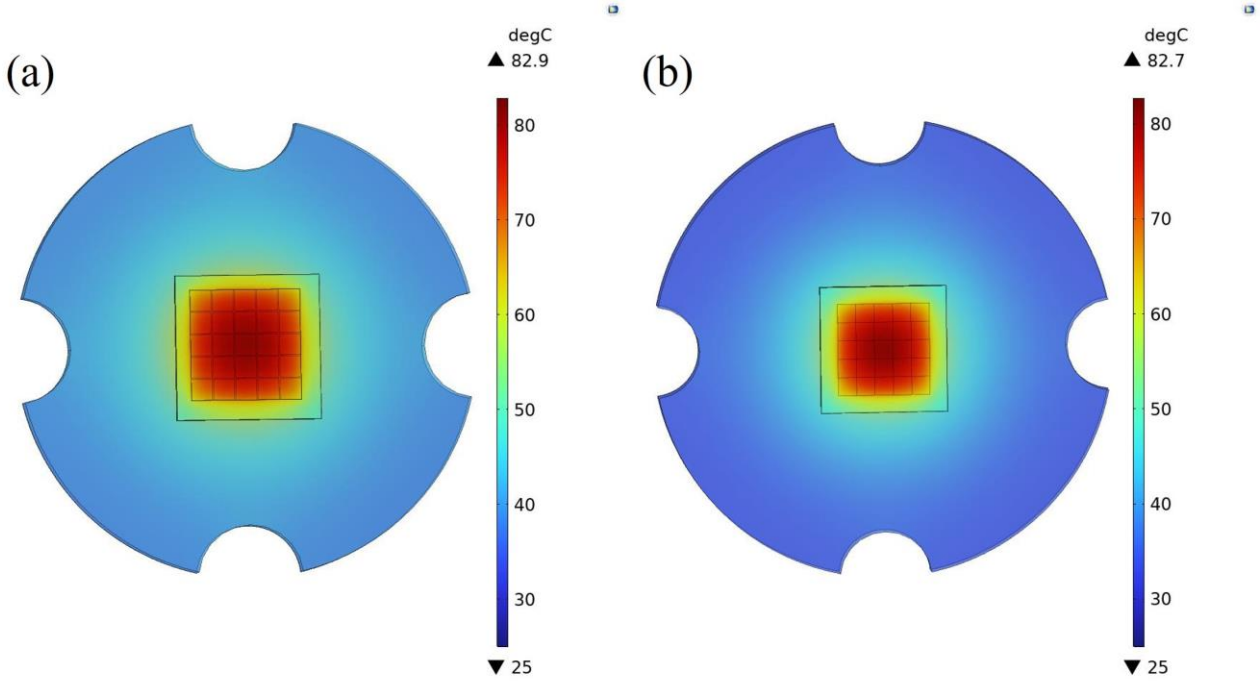

Figure 14. Simulation at 170 W thermal power: (**a**) 35 mm; (**b**) 40 mm.

5. Conclusions

This study conducts a comprehensive analysis of how copper substrate area (diameters of 20 mm, 25 mm, and 32 mm) affects the optoelectronic and thermal properties of 400 W high-power LED devices. The experimental results demonstrate that increasing

the substrate area significantly improves both optical output and thermal performance. Specifically, compared to the 20 mm substrate, the 32 mm substrate achieves approximately 20% higher blue optical power and 15% higher white luminous flux. At a driving current of 70 A, the maximum chip temperature is reduced from 115 °C to 85.7 °C, with substantially improved temperature uniformity. White LEDs exhibit more pronounced temperature-dependent degradation in voltage and luminous output due to thermal quenching of the phosphor layer. Through COMSOL-based simulations extended to 35 mm and 40 mm substrates, it is observed that the thermal enhancement tends to saturate beyond 35 mm, with only a marginal further improvement at 40 mm. Considering the balance between performance gains and material costs, 35 mm is identified as the optimal substrate size for this device configuration.

This study validates the strong agreement between simulation and experimental data, confirming the reliability of the modeling approach. These findings offer practical guidance for substrate design and thermal management in high-power, high-density LED applications, supporting both performance optimization and cost-effective development.

Author Contributions: Y.M. constructed the model, collected the data, and authored the manuscript; C.X. contributed to designing research and edited the manuscript; X.L., Y.T. and H.Y. assisted with manuscript writing and analysis of specific experimental findings; X.Y. conducted the simulation, performed experiments, and measured the model; B.L. and J.D. conceived the initial concept and oversaw the project. All authors have read and agreed to the published version of the manuscript.

Funding: This research was financially supported by the Key Technologies Innovation and Industrialization Projects of Fujian Province (Grant No. 2023QX007) and the Industry-University-Research Cooperation Project of Fujian Science and Technology Department (Grant No. 2023H6018).

Institutional Review Board Statement: Not applicable.

Informed Consent Statement: Not applicable.

Data Availability Statement: Data are contained within the article.

Conflicts of Interest: The authors declare no conflicts of interest.

Abbreviations

The following abbreviations are used in this manuscript:

BMs	Base Materials
LED	Light-Emitting Diode
MCPCB	Metal Core Printed Circuit Board
MOSFET	Metal-Oxide-Semiconductor Field-Effect Transistor
TIMs	Thermal Interface Materials

References

1. Matic, M.; Andr, O.; Pri, S. Measuring System for Determining the Quality of LED Light Sources and an Overview of LED Light Bulbs for Household Use. *Sensors* **2022**, *22*, 8351. [CrossRef]
2. Ibrahim, M.S.; Jing, Z.; Yung, W.K.; Fan, J. Bayesian based lifetime prediction for high-power white LEDs. *Expert Syst. Appl.* **2021**, *185*, 115627. [CrossRef]
3. Schirripa Spagnolo, G.; Satta, G.; Leccese, F. LEDs for Underwater Optical Wireless Communication. *Photonics* **2025**, *12*, 749. [CrossRef]
4. Liu, Z.; Ren, K.; Dai, G.; Zhang, J. A Review on Micro-LED Display Integrating Meta surface Structures. *Micromachines* **2023**, *14*, 32–33.
5. Leong, M.F.; Scott, S. Lighting Safety Considerations. *IEEE Trans. Ind. Appl.* **2015**, *51*, 4233–4238. [CrossRef]
6. Ke, X.; Wang, X.; Qin, H.; Liang, J. Experimental Study on Chromaticity Control in Visible Light Communication Systems. *Photonics* **2023**, *10*, 1013. [CrossRef]

7. Li, J.; Pan, C.; Pan, J.; Lin, J.; Lu, M.; Jiang, Z.L.; Fang, J. Long-Distance, Real-Time LED Display-Camera Communication System Based on LED Point Clustering and Lightweight Image Processing. *Photonics* **2022**, *9*, 721.
8. Hel, D.; Thom, W.; Fra, K. Short-Wave Ultraviolet-Light-Based Disinfection of Surface Environment Using Light-Emitting Diodes: A New Approach to Prevent Health-Care-Associated Infections. *Microorganisms* **2023**, *11*, 386.
9. Sam, K.; Gop, S.K.M. Cooling of High-Power LEDs by Liquid Sprays: Challenges and Prospects. *Appl. Therm. Eng.* **2021**, *184*, 115640. [CrossRef]
10. Saa, I.; Dou, O.; Sam, I.B.; Arao, Z.; Char, K.; Asse, A.; Canale, L. Optimal Thermal Management Using the Taguchi Method for LED Lighting Squared Heat Sink, Including Statistical Approaches. *Sustainability* **2025**, *17*, 1811. [CrossRef]
11. Zhang, J.; Yang, D.; Wang, X.; Qu, J.; Gao, W. Development and numerical optimization of a cylindrical wire-fin-type integrated ionic wind heat sink for cooling high-power LEDs. *Int. J. Heat Fluid Flow* **2024**, *109*, 109527.
12. Li, S.; Liu, J.; Ding, L.; Liu, J.; Xu, J.; Peng, Y.; Chen, M. Active Thermal Management of High-Power LED Through Chip on Thermoelectric Cooler. *IEEE Trans. Electron. Devices* **2021**, *68*, 1753–1756. [CrossRef]
13. Ding, X.; Tang, Y.; Li, Z. Thermal and optical investigations of high power LEDs with metal embedded printed circuit boards. *Int. Commun. Heat Mass Transf.* **2015**, *66*, 32–39. [CrossRef]
14. Wu, Y.; Sun, Z.; Liu, N.; Wang, Z.; Hu, Y.; Bai, T.; Wang, T.; Chen, J.; Qiu, X.; Zhang, X.; et al. Controlled Growth of Graphene-Skinned Al_2O_3 Powders by Fluidized Bed-Chemical Vapor Deposition for Heat Dissipation. *Adv. Sci.* **2025**, *12*, e03388. [CrossRef]
15. Kyatam, S.; Rodrigues, L.; Maslovski, S.; Alves, L.N.; Mendes, J.C. Improving the reliability of power LEDs with diamond boards. *Diam. Relat. Mater.* **2022**, *127*, 109144. [CrossRef]
16. Baek, S.-H.; Choi, D.-C.; Kim, Y.S.; Na, H.; Lee, S.-N. The Correlation between Surface V-Shaped Defects and Local Breakdown Phenomena in GaN-Based LEDs. *Photonics* **2023**, *10*, 1103.
17. Wang, S.L.; Xiong, C.B.; Tang, Y.W.; Li, X.Z.; Liu, Q. Effect of the number and position of eutectic chips on the luminescence performance of ceramic eutectic package LED. *J. Lumin.* **2020**, *41*, 1421–1430.
18. Li, X.Z.; Xiong, C.B.; Tang, Y.W.; Hao, D.H. High power flip LED chip ceramic package device top surface micro-luminous uniformity. *J. Lumin.* **2021**, *42*, 1436–1445.
19. Liu, Q.; Xiong, C.B.; Tang, Y.W. Influence of multi-core CSP-LED chip spacing on thermal congestion. *J. Lumin.* **2020**, *41*, 308–315.
20. Huang, L.F.; Xiong, C.B.; Tang, Y.W.; Yuan, H.; Ma, Y.H.; Yang, X.Y. Effect of copper substrate area, solder and conductive copper foil thickness on the ultimate photoelectric performance of high power density LED. *J. Lumin.* **2024**, *45*, 1196–1210.
21. Chen, Q.; Ma, Y.; Yu, X.; Hu, R.; Luo, X. Phosphor Temperature Overestimation in High-Power Light-Emitting Diode by Thermocouple. *IEEE Trans. Electron. Devices* **2017**, *64*, 463–466. [CrossRef]
22. Guo, L.F.; Wang, Z.X.; Zhou, Y.Q. Unity emission in organic phosphonium antimony halide for high color rendering white LED. *J. Lumin.* **2024**, *266*, 120326.
23. Li, Y.; Ma, C.; Zuo, C.; Ye, W.; Shen, X.; Wang, Y.; Li, Y.; Zhao, C.; Wen, Z.; Yuan, X.; et al. High thermal stability AlN-YAG: Ce composite phosphor ceramics for high-power laser-driven lighting. *Appl. Phys. Lett.* **2021**, *119*, 251903.

Disclaimer/Publisher's Note: The statements, opinions and data contained in all publications are solely those of the individual author(s) and contributor(s) and not of MDPI and/or the editor(s). MDPI and/or the editor(s) disclaim responsibility for any injury to people or property resulting from any ideas, methods, instructions or products referred to in the content.